

Article

# Unravelling the Supramolecular Driving Forces in the Formation of CO<sub>2</sub>-Responsive Pseudopeptidic Low-Molecular-Weight Hydrogelators

Ferran Esteve <sup>1</sup>, Alexis Villanueva-Antolí <sup>2</sup>, Belén Altava <sup>1,\*</sup>, Eduardo García-Verdugo <sup>1</sup>  
and Santiago V. Luis <sup>1,\*</sup>

<sup>1</sup> Departamento de Química Inorgánica y Orgánica, Universitat Jaume I, Av. Sos Baynat s/n, 12071 Castelló de la Plana, Spain; estevef@uji.es (F.E.); cepeda@uji.es (E.G.-V.)

<sup>2</sup> Institute of Advanced Materials (INAM), Universitat Jaume I, 12071 Castelló de la Plana, Spain; aantoli@uji.es

\* Correspondence: altava@uji.es (B.A.); luiss@uji.es (S.V.L.)

**Abstract:** A new family of C<sub>2</sub>-symmetric pseudopeptides with a high functional density for supramolecular interactions has been synthesized through the attachment of four amino acid subunits to a diamino aliphatic spacer. The resulting open-chain compounds present remarkable properties as low-molecular-weight hydrogelators. The self-assembled 3D networks were characterized by SEM analyses, observing regular nanofibres with 80–100 nm diameters. Spectroscopic and molecular modelling experiments revealed the presence of strong synergic effects between the H-bonding and  $\pi$ - $\pi$  interactions, with the best results obtained for the homoleptic tetra-pseudopeptide derived from L-Phe. In addition, these bioinspired hydrogels possessed pH- and CO<sub>2</sub>-responsive sol-gel transitions. The formation of ammonium carbamate derivatives in the presence of carbon dioxide led to a detrimental change in its adequate self-assembly. CO<sub>2</sub> desorption temperatures of ca. 70 °C were assigned to the thermodynamically favoured recovery of the supramolecular gel.

**Keywords:** pseudopeptides; hydrogels; LMWG; supramolecular chemistry; responsive materials; CO<sub>2</sub> absorption



**Citation:** Esteve, F.; Villanueva-Antolí, A.; Altava, B.; García-Verdugo, E.; Luis, S.V. Unravelling the Supramolecular Driving Forces in the Formation of CO<sub>2</sub>-Responsive Pseudopeptidic Low-Molecular-Weight Hydrogelators. *Gels* **2022**, *8*, 390. <https://doi.org/10.3390/gels8060390>

Academic Editors: Hailei Zhang and Yonggang Wu

Received: 2 June 2022

Accepted: 17 June 2022

Published: 20 June 2022

**Publisher's Note:** MDPI stays neutral with regard to jurisdictional claims in published maps and institutional affiliations.



**Copyright:** © 2022 by the authors. Licensee MDPI, Basel, Switzerland. This article is an open access article distributed under the terms and conditions of the Creative Commons Attribution (CC BY) license (<https://creativecommons.org/licenses/by/4.0/>).

## 1. Introduction

Soft materials based on low-molecular-weight gelators (LMWG) have received significant attention in the last two decades, as they present some interesting features such as well-defined molecular weights, easy structural tuneability, and their capacity to form relatively regular nanostructures [1–4]. The strength of their 3D networks, and thus, the critical gelation concentration (CGC) of the corresponding supramolecular gels, is extremely dependent on the intermolecular non-covalent interactions present [5–7].

Gels formed in aqueous systems, i.e., hydrogels, are of special interest due to the wide variety of applications possible, ranging from tissue engineering [8,9] and controlled drug delivery [10–12] to nanoscale electronics [13] and actuators [14,15]. Hydrogelators based on amino acids are very attractive because of the highly tuneable characteristics of the amino acid fragments, their natural origin, and, accordingly, their potential for biocompatibility and biodegradability [16–21].

In this regard, C<sub>2</sub>-symmetric pseudopeptidic compounds displaying apolar spacers have shown remarkable gelating behaviours in different solvents [22], with the presence of additional functional components, such as urea fragments, significantly increasing the stability of the resulting supramolecular gels [23,24]. The introduction of polar functionalities in such pseudopeptides with apolar spacers has shown to afford efficient hydrogelators with pH-responsive self-assembling properties [25]. These results highlight the potential of using pseudopeptides as gelators due to the high flexibility of design that such molecules

offer. Related approaches have allowed, for instance, the development of bioinspired hydrogels as controlled drug release systems [26].

Upon exposure to external stimuli, the dynamic nature of the different intermolecular interactions involved in the formation of a polymeric supramolecular structure enables reversible sol–gel transitions [27–30]. Unsurprisingly, many efforts have been devoted to the design of hydrogels that exhibit promising switchable properties on the basis of their different applications [31–33]. In this regard, CO<sub>2</sub> is an ideal candidate for acting as a stimulus because it is a non-toxic, cheap, and abundant species. Therefore, several CO<sub>2</sub>-switchable soft materials have been precisely designed, leading to interesting advantages in the fields of chemosensors, absorbents, and drug delivery [34–39]. Nevertheless, the vast majority of the amino-based reported systems describe either the use of polymeric materials or the design of CO<sub>2</sub>-promoted LMWGs that are only suitable for gelation in organic solvents, thus hampering their use in biological applications [40]. An additional hurdle of amine-containing CO<sub>2</sub> absorbents is the large energy consumption associated with the high temperatures required for desorption, stressing the need for the development of more efficient systems [41].

Taking these inspiring precedents into account, we report herein the preparation of open-chain C<sub>2</sub>-symmetric pseudopeptides containing four amino acid units within their structure. These simple compounds can be used to generate stable hydrogels in which self-assembly is governed by  $\pi$ – $\pi$  interactions and H bonding [42,43]. The resulting supramolecular materials display promising properties for reversible, CO<sub>2</sub>-controlled hydrogelation. They present a rapid and isothermal CO<sub>2</sub> absorption at room temperature, with subsequent CO<sub>2</sub> desorption from the resulting ammonium carbamate derivative upon heating at temperatures of <80 °C, which defines a change in the self-assembly process.

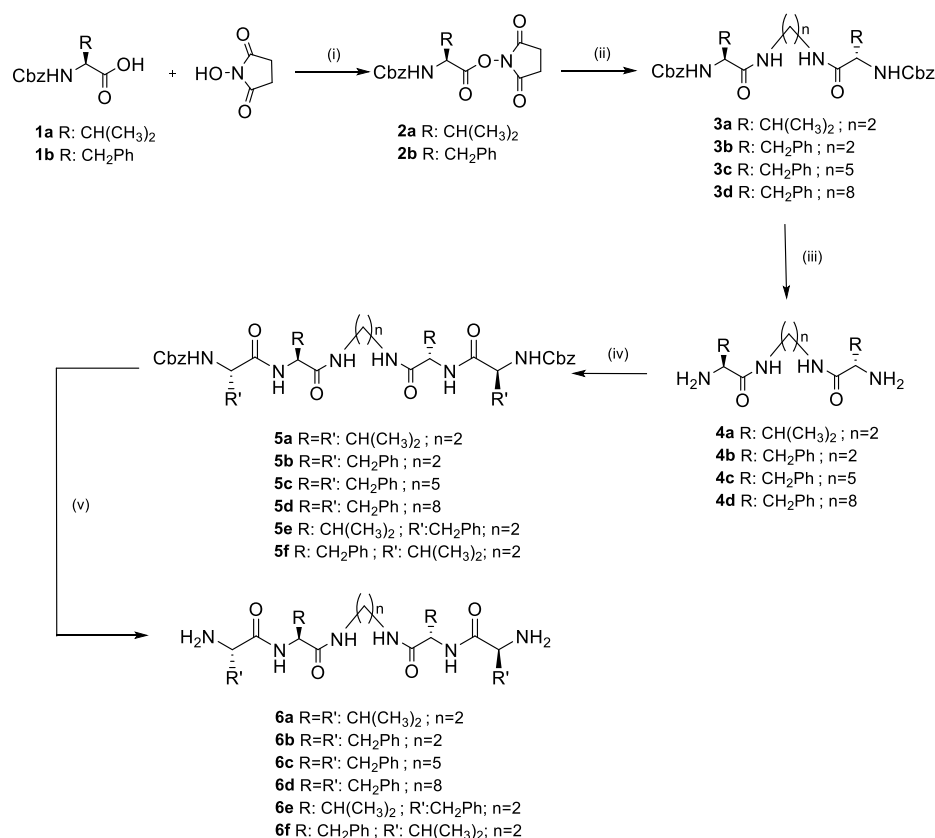
## 2. Results and Discussion

### 2.1. Synthesis of the Pseudopeptidic Compounds and Gelation Properties of LMWGs

The synthesis of the different C<sub>2</sub>-symmetric tetra-pseudopeptides, **6a–f**, is shown in Scheme 1. Compounds **4a–d** were obtained following the previously reported synthetic procedure (Scheme 1) [44].

Briefly, the first step consisted of the synthesis of the activated esters of the L-amino acids, using DCC as the coupling agent. The resulting activated esters, **2a,b**, were reacted with the desired diamine to yield the N-Cbz-protected pseudopeptides, **3a–d**. The deprotection step to create the compounds **4a–d** relied on the use of a HBr/Hac (33%) solution. An additional coupling step with either **2a** or **2b** resulted in the N-protected tetra-pseudopeptides **5a–f**. The subsequent hydrogenation in the presence of palladium on activated carbon led to the desired deprotected tetra-pseudopeptides **6a–f**. The overall yields to produce **6a–f** from compounds **1a,b** ranged from 20% to 40%.

The gelation properties of the tetra-pseudopeptidic compounds **6a–f** were assayed in different aqueous mixtures and in water. As shown in Table 1, the nature of the amino acid side chain played a critical role in the self-assembly behaviour. As a matter of fact, the phenylalanine derivative **6b** formed gels in water mixtures and in water at 1 mg/mL (entries 2, 17, and 20, Table 1), while the valine-derived compound **6a** was not able to yield hydrogels under analogous conditions (entries 1, 18, and 19, Table 1). These results suggested that  $\pi$ – $\pi$  interactions could be a major requirement for the 3D network to grow. Interestingly, when the gelation properties for compound **6b** were assayed in H<sub>2</sub>O:DMSO (90:10, *v/v*), an instantaneous gelation process was observed without the need for any external stimuli. On the other hand, when the experiments were performed in EtOH:H<sub>2</sub>O mixtures, sonication was always needed to obtain similar hydrogels.



**Scheme 1.** The synthesis of tetra-pseudopeptidic compounds. (i) DCC, 0 °C, 16 h; (ii) dry DME, ethylene diamine/1,5-diaminopentane/1,8-diaminooctane, r.t., 18 h; (iii) HBr/HAc (33%), 3 h/liquid-liquid extraction at pH = 10; (iv) dry DME, 2, r.t., 18 h; and (v) H<sub>2</sub>, Pd/C, MeOH. All schemes follow the same formatting.

**Table 1.** Gelation properties of compounds **6a–f** in aqueous solutions <sup>1</sup>.

Entry	Comp.	Solvent(s)	Proportion (v/v)	Conc. (mg/mL)	Result
1	<b>6a</b>	H <sub>2</sub> O:DMSO	90:10	1	S
2	<b>6b</b>	H <sub>2</sub> O:DMSO	90:10	1	G <sup>4</sup>
3	<b>6c</b>	H <sub>2</sub> O:DMSO	90:10	1	wG <sup>4</sup>
4	<b>6c</b>	H <sub>2</sub> O:DMSO	90:10	3	G <sup>4</sup>
5	<b>6d</b>	H <sub>2</sub> O:DMSO	90:10	1	wG <sup>2</sup>
6	<b>6d</b>	H <sub>2</sub> O:DMSO	90:10	5	wG <sup>3</sup>
7	<b>6e</b>	H <sub>2</sub> O:DMSO	90:10	1	S
8	<b>6e</b>	H <sub>2</sub> O:DMSO	90:10	5	S
9	<b>6f</b>	H <sub>2</sub> O:DMSO	90:10	1	S
10	<b>6f</b>	H <sub>2</sub> O:DMSO	90:10	5	wG <sup>3</sup>
11	<b>6e + 6f</b>	H <sub>2</sub> O:DMSO	90:10	0.5 + 0.5	wG
12	<b>6b</b>	H <sub>2</sub> O:DMSO	50:50	1	wG <sup>3</sup>
13	<b>6a</b>	H <sub>2</sub> O:EtOH	90:10	1	I
14	<b>6b</b>	H <sub>2</sub> O:EtOH	90:10	1	I
15	<b>6b</b>	H <sub>2</sub> O:EtOH	70:30	1	wG <sup>3</sup>
16	<b>6b</b>	H <sub>2</sub> O:EtOH	70:30	0.5	wG <sup>3</sup>
17	<b>6b</b>	H <sub>2</sub> O:EtOH	50:50	1	G <sup>3</sup>
18	<b>6a</b>	H <sub>2</sub> O:EtOH	50:50	1	S
19	<b>6a</b>	H <sub>2</sub> O	-	1	I <sup>2</sup>
20	<b>6b</b>	H <sub>2</sub> O	-	1	G <sup>2</sup>

<sup>1</sup> The gel formation was qualitatively analysed by the vial inversion technique. I: insoluble, S: soluble, wG: weak gel, and G: gel. <sup>2</sup> Heating at 90 °C for 5 min. <sup>3</sup> Ultrasonication for 5 min. <sup>4</sup> Instantaneous formation of gel.

The key role of aromatic interactions in the aggregation capacity of these pseudopeptides was confirmed by the results obtained for the heteroleptic compounds **6e** and **6f**, which contained only two aromatic groups in their side chains instead of the four displayed by **6b**. When 1 mg of **6e** or **6f** was dissolved in H<sub>2</sub>O:DMSO (90:10, *v/v*), a clear solution was obtained, thus revealing a lower gelating ability (entries 7 and 9, Table 1). When the concentration of the heteroleptic compounds was increased to 5 mg/mL, this triggered the formation of a weak hydrogel for **6f** (entry 10, Table 1), whereas the **6e** sample still appeared as a clear solution (entry 8, Table 1). Interestingly, a weak gel was obtained when equimolar amounts of **6e** and **6f** (0.5 mg/mL each) were mixed, inferring that the two-component mixture was able to self-assemble in fibrillar aggregates (entry 11, Table 1). In view of these results, we also explored the hydrogelation properties of the precursors **4a–4e**, although their extremely low solubility in water hampered this approach.

In addition, the effect of the aliphatic spacer length on the gelation ability was also evaluated. Previous studies on related pseudopeptides have demonstrated that, depending on the length of the alkyl aliphatic spacer, the amide groups can be in *-syn* or *-anti* disposition [45], which affects their self-assembly behaviour. Dissolving 1 mg of **6c**, which has three additional methylene groups in the spacer relative to **6b**, in 100  $\mu$ L of DMSO and adding 900  $\mu$ L of water led to the formation of a weak gel upon sonication. In order to obtain a stronger gel, 3 mg of **6c** was required (entries 3 and 4, Table 1). Compound **6d**, which contained an even longer spacer ( $n = 8$ ), was only able to promote the formation of weak gels, even at 5 mg/mL (entries 5 and 6, Table 1). Thus, the compound with the shortest aliphatic spacer ( $n = 2$ ), **6b**, presented the best gelation properties in aqueous media, most likely as a direct result of the optimal preorganization of the aromatic moieties of the side chains. SEM experiments provided additional insights into the microstructure of the hydrogels. Thus, SEM images for the dried gel of **6b** that was obtained in H<sub>2</sub>O:DMSO (90:10 *v/v*) allowed the presence of a well-defined interpenetrated network of regular nanofibers, displaying diameters of 80–100 nm, to be observed (Figure 1a–c) [46].

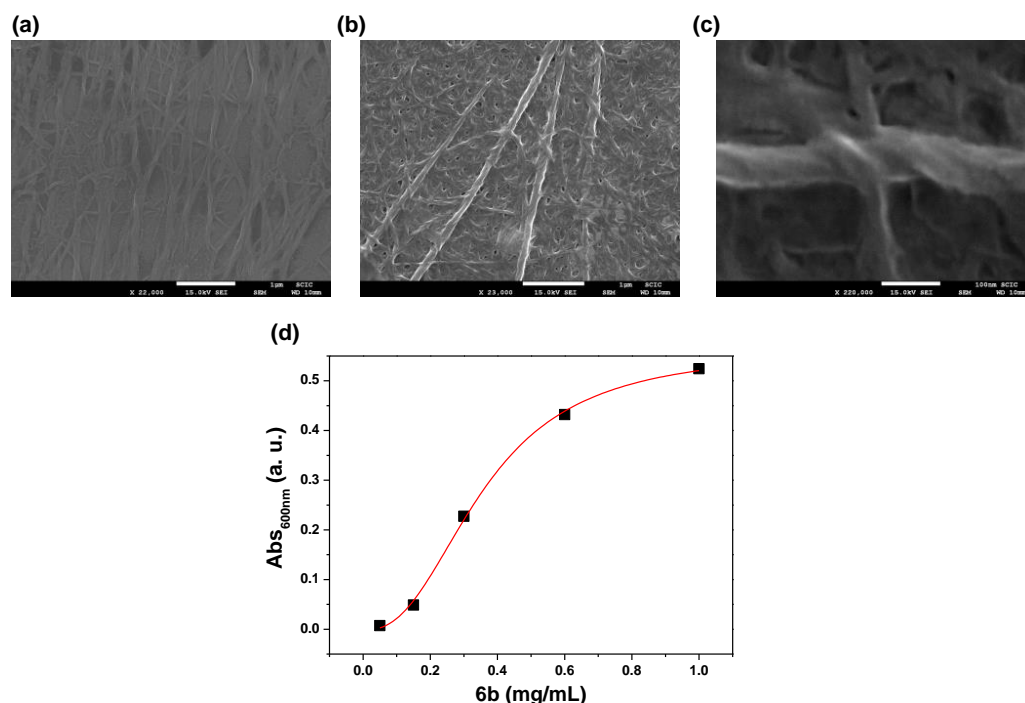


**Figure 1.** (a–c) SEM images for the dried sample of **6b** (1 mg/mL) in DMSO:H<sub>2</sub>O (10:90) and (d) UV absorption at 600 nm for **6b** at different concentrations in H<sub>2</sub>O:DMSO (90:10) [26]. The red line corresponds to the sigmoidal fitting calculated using Origin Software.

Vial inversion analyses allowed for the quantification of the critical gelation concentration (CGC), which is defined as the minimum amount of gelator required to gelate 1 mL of solvent at a given temperature [12]. The data presented in Table S1 permitted the assignment of a CGC lower than 0.6 mg/mL for compound **6b** (see Figure S1). This value demonstrated the remarkable gelation properties of **6b**, which belongs to the class of superhydrogelators [47]. UV-VIS spectroscopy was also used to determine the CGC for **6b** (Figure 1d). The formation of the gel could be straightforwardly monitored by measuring the absorption changes at 600 nm. A sigmoidal curve was observed with an inflexion point at ca. 0.4 mg/mL. This concentration was in good agreement with the value determined by the vial inversion method.

The thermal stability of the gel formed from **6b** (H<sub>2</sub>O:DMSO (90:10 *v/v*), 1 mg/mL) was likewise investigated using the vial inversion test (Table S2). The hydrogel was stable until 85 °C, at which point the soft material started to lose its viscosity. This finding was attributed to some evaporation of the water present in the initial solvent mixture. The mechanical properties of this hydrogel (H<sub>2</sub>O:DMSO (90:10 *v/v*)) were studied using rheological measurements. A typical LMWG presents a storage and a loss modulus ( $G'$  and  $G''$ , respectively) which are frequency independent, and will break under relatively low strain [48]. Figure 2 displays the rheological results obtained for **6b** (1 mg/mL). The storage modulus ( $G'$ ) of the gel was much higher than the loss modulus ( $G''$ ) over the whole range of the frequency sweep, which is characteristic of gel-like materials (Figure 2a). The strain sweep measurement (Figure 2b) showed that both the storage and loss moduli of the gel remained constant up to 10 Pa of stress (3.6% strain), corresponding to the so-called linear viscoelastic region (LVER). Furthermore, the average complex viscosity of the hydrogel was quantified, obtaining a value of 113 Pa·s. The complex viscosity dependence with the angular frequency was also evaluated, observing a linear relationship with the expected negative slope (Figure 2c). By heating the sample prepared in situ on the Peltier geometry, it was possible to evaluate the effect of temperature on the mechanical properties of the pseudopeptidic soft material. For instance, by observing the complex viscosity trend with temperature, a linear range was obtained from 25 to 85 °C (Figure 2d). When the temperature reached values higher than 83 °C, a clear decrease in the viscosity was observed, indicating that the sample was losing its gel-like properties. Hence, the critical gelation temperature (CGT) was identified as 83 °C, which is a value within the same range obtained by the vial inversion method (see Table S2). This material can be classified as a thixotropic gel because, upon shaking the vial, the sample became much more fluid than in its static state; furthermore, after resting the vial for 24 h, the gel could be restored. The same rheological experiments were also performed for **6b** at higher gelator concentrations (5 mg/mL in H<sub>2</sub>O:DMSO (90:10 *v/v*)). Not surprisingly, the resulting gel demonstrated a higher complex viscosity, with an average value of 1640 Pa·s, and higher  $G'$  and  $G''$  values. This stronger gel was able to resist oscillation strains of ca. 40 Pa, corroborating the tougher properties of the gel at higher concentrations (Figure S2).

Next, we decided to analyse whether an external stimulus could induce a gel–sol transition [49]. Considering the functional groups present in the chemical structure of **6b**, the pH appeared to be a good candidate, as the pseudopeptide presented terminal amino groups (basic) and amide groups (slightly acidic). Therefore, vial inversion tests were carried out on the samples at different pH values, which were controlled by commercially available buffers (Figure S3). The results, presented in Table 2, revealed that the higher the pH was, the more favourable was the formation of the gel. It must be mentioned that the chemical structure of the LMWG was very stable and was not expected to degrade under the assayed conditions. Notwithstanding, these kinds of compounds have been observed to degrade by proteases under biological conditions, which represents an interesting feature in terms of their biodegradability [26].

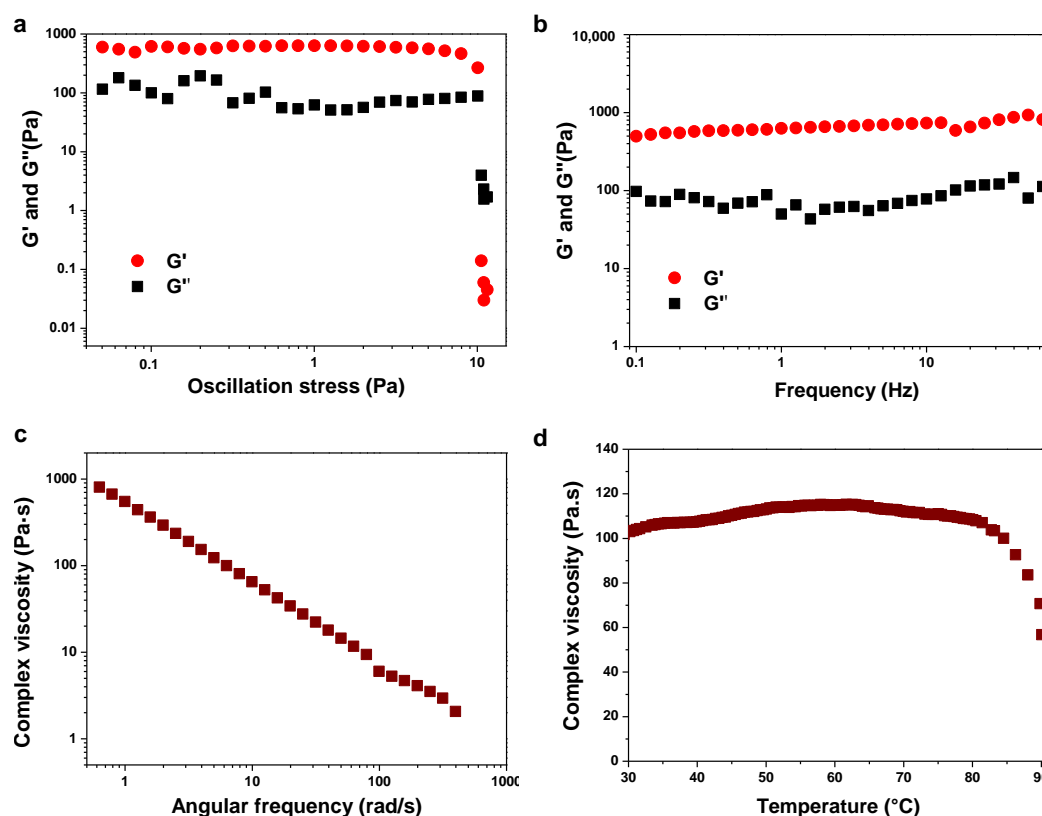


**Figure 2.** Rheological measurements for the hydrogel formed from **6b** (1 mg/mL, H<sub>2</sub>O:DMSO (90:10 *v/v*)). (a) Amplitude sweeps with 1 Hz at 25 °C; (b) frequency sweeps with 0.1 Pa strain at 25 °C; (c) complex viscosity vs. angular frequency; and (d) the dependence of the complex viscosity on the temperature using a heating rate of 0.2 °C/min and a constant frequency of 1 Hz and 0.1% strain.

**Table 2.** Gelation properties as a function of pH for **6b** (1 mg/mL) in H<sub>2</sub>O:DMSO (90:10 *v/v*).

Vial	Buffer (mM)	pH	Result <sup>1</sup>
1	- <sup>2</sup>	1.2	S
2	Citrate (20)	4.4	wG
3	Citrate (20)	6.0	wG
4	Phosphate (30)	7.1	wG
5	HEPES (20)	8.1	G

<sup>1</sup> Gel formation was qualitatively analysed by the vial inversion technique. <sup>2</sup> The sample at pH = 1 was prepared by adding 20 µL of concentrated HCl. S: soluble, wG: weak gel, and G: gel. The buffers were commercially available and, when needed, the pH was adjusted using NaOH or HCl. See Figure S3 for the results of the vial inversion tests.

These pH-dependent results indicated the participation of the terminal amino groups in the formation of the non-covalent network, since when these groups were in their fully protonated form, a completely transparent solution was obtained. Interestingly enough, some crystallization could be observed in the sample at a pH of 1 after aging the vial for one week. The SEM images of the resulting crystalline solid revealed the formation of fibre-like crystals, which were likely the result of the formation of diprotonated ammonium salts for **6b** (Figure S4). Therefore, the protonation of the primary amines led to a soluble ammonium salt that hampered the formation of the 3D supramolecular network. It must be noted, however, that **6b** was able to form weak gels even at a physiological pH (Table 2, vial 4), which opens a wide scope for future applications in areas such as drug delivery.

## 2.2. Supramolecular Driving Forces

To obtain relevant information about the supramolecular interactions that governed the formation of these soft materials, a series of  $^1\text{H}$  NMR and theoretical studies were undertaken. First of all, increasing amounts of water were added to a 3 mM solution of **6b** in  $\text{DMSO-}d_6$ , and  $^1\text{H}$  NMR spectroscopy was used to observe some relevant changes in the characteristic signals of the pseudopeptide. Indeed, most of the peaks of **6b** broadened with the addition of water, suggesting the formation of oligomeric aggregates. An upfield shift was observed for the proton signals of the central amide groups (green triangles in Figure 3), indicating a different involvement of hydrogen bonding in the supramolecular aggregates.

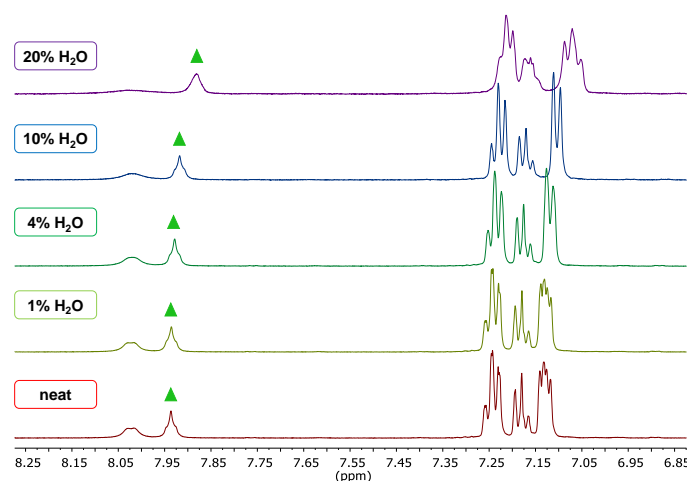


**Figure 3.** Partial  $^1\text{H}$  NMR (500 MHz,  $\text{DMSO-}d_6$ ) spectra for the titration of **6b** (3 mM) with increasing amounts of water. The water content is indicated as  $v/v$  (%). The signal for the central amide groups has been marked with green triangles.

In a similar manner, the protons corresponding to the aromatic moieties experienced a shift towards a lower  $\delta$ . This was especially noticeable for the protons assigned to the aromatic ring of the central amino acid scaffolds, suggesting their participation in hydrophobic interactions. In addition, the methylene protons of the aliphatic central spacer and the benzylic protons also experienced a different electronic environment in the aggregates, as evidenced by the upfield shift for the central methylene protons (orange discontinuous lines, Figure S5).

In terms of the signals for the protons of the water molecules, a progressive downfield evolution could be observed, shifting from 3.35 to 3.93 ppm ( $\Delta\delta = +0.58$  ppm) when the amount of water reached 20%  $v/v$  (purple discontinuous lines, Figure S5). This change in the electronic environment was likely the result of water entrapment in the three-dimensional network that was formed, thus increasing the H bonding. Interestingly, analogous experiments performed for **6f** revealed less-pronounced shifts for both the water molecules and the signals from the heteroleptic pseudopeptide (Figures S6 and S7). As a matter of fact, the signal for water shifted by  $\Delta\delta = +0.28$  ppm. Although the aromatic protons of **6f** also shifted towards lower  $\delta$  values in the presence of water, this shift was much less significant than the one observed for **6b** (Figure S7). This indicates that the homoleptic tetra-phenylalanine-derived pseudopeptide promoted higher efficiencies in forming the supramolecular aggregates, in good accordance with the trends found in gelation studies (see, for instance, entries 2 and 9, Table 1).

Variable-temperature  $^1\text{H}$  NMR experiments corroborated the fundamental role of intermolecular hydrogen-bonding and  $\pi$ - $\pi$  interactions in the self-assembly of the pseudopeptides. Important conformational information was gathered when a sample containing a 3 mM solution of **6b** in  $\text{H}_2\text{O:DMSO}$  (20:80) was heated from 30 to 80  $^\circ\text{C}$ . As expected, the proton signals of the amide groups and water experienced an upfield shift as the

temperature increased (*ca.*  $\Delta\delta = -0.24$  and  $-0.35$  ppm for  $\text{NH}_{\text{amide}}$  and  $\text{H}_2\text{O}$ , respectively), suggesting their participation through hydrogen-bonding interactions within the supramolecular network of aggregates (Figures 4a and S8).

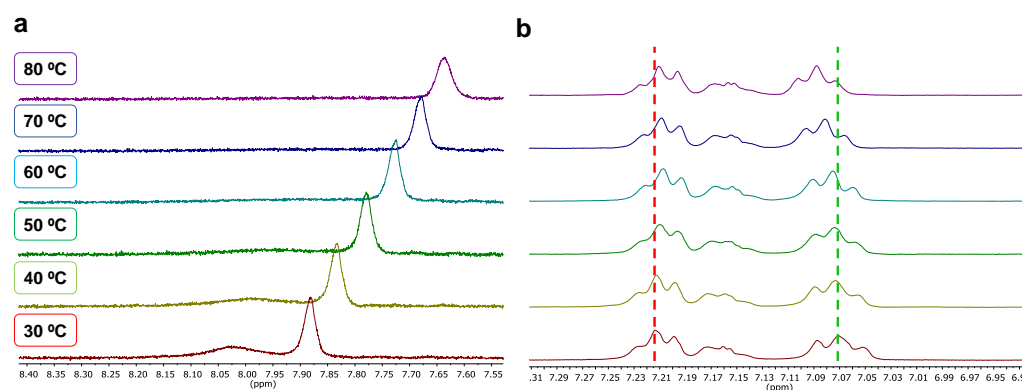


**Figure 4.** Partial  $^1\text{H}$  NMR (500 MHz,  $\text{DMSO-}d_6$ ) spectra for the variable-temperature experiments of **6b** (3 mM,  $\text{H}_2\text{O}:\text{DMSO}$ , 20:80); (a) amide group region and (b) aromatic region.

A different scenario was observed on behalf of the signals for the aromatic units. The multiplet appearing at 7.21 ppm underwent a minor upfield shift, as marked with a discontinuous red line in Figure 4b. On the other hand, a more pronounced change was noted for the signal appearing at 7.07 ppm at 30 °C, but with the opposite direction than the one found at 7.21 ppm. This trend is in good agreement with interconnected  $\pi$  systems, where one of the aromatic units acts as the  $\pi$ -donor and the other one as the  $\pi$ -acceptor [50]. Additionally, the protons of the chiral carbon centres, the methylene protons of the central spacer, and the benzylic protons experienced a small shift ( $\Delta\delta = +0.03$  ppm, discontinuous orange lines, Figure S8).

Molecular modelling for **6b**, **6e**, and **6f** unravelled the importance of synergic  $\pi$ - $\pi$  interactions, which were only observed in the case of **6b**. All the models were based on the molecular mechanics at the MMFFaq level of theory, taking into account the water solvation (see experimental section for more details). The most stable conformation for the dimeric species was calculated as a simple model to surmise whether each pseudopeptide could form larger aggregates by means of non-covalent forces. The modeled structures for the tetra-pseudopeptidic dimers revealed noteworthy disparities. For instance, the two modeled molecules of **6b** adopted a  $\beta$ -sheet spatial disposition that was stabilized by means of intermolecular hydrogen bonds involving the central amide groups of the pseudopeptidic scaffolds. Additionally, the hydrophobic aromatic units were located in the outer part of the molecules, intermolecularly interacting through  $\pi$ - $\pi$  forces (Figure 5a). Therefore, the adopted conformation allowed for the construction of bigger self-assembled supramolecular structures, leading to the formation of fibre-like aggregates (Figure 5d). On the other hand, the modeled dimers for the heteroleptic tetra-pseudopeptides rather embraced a tangled conformation, only stabilized through intermolecular hydrogen bonding between the amide groups, which precluded an efficient extension of the network to form gels (Figure 5b,c,e).

The non-covalent interactions governing the gel formation for **6b** were studied in greater detail. The four amide groups (presenting with an *-anti* disposition) of each of the pseudopeptidic molecules were highly interconnected with the analogues of the neighbouring molecule, leading to the formation of parallel hydrogen bonds (Figure S9a). The average distance between the  $\text{O}\cdots\text{N}$  atoms involved in the interaction was 2.780 Å (90%  $\text{vdW}_{\text{N,O}}$ ) [51], suggesting a strong interaction even in a competitive polar medium. In terms of the hydrophobic interactions between the dimeric species, four different intermolecular edge-to-face  $\pi$ - $\pi$  interactions were detected (Figure S9b). In addition, weak intramolecular  $\text{NH}\cdots\pi$  forces were identified between the phenyl rings of the phenylalanine side

chains and the acidic NH proton of the amide groups, further stabilising the whole system (Figure S9c) [52].

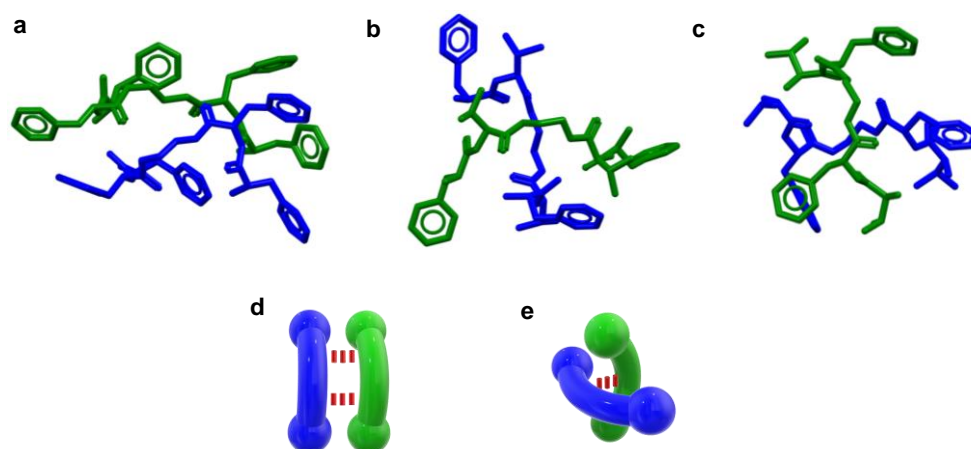


**Figure 5.** The most stable conformations (Spartan08', MMFFaq) obtained for the dimers of (a) **6b**, (b) **6e**, and (c) **6f**; (d) a representation of the parallel  $\beta$ -sheet; and (e) the tangled dimeric assemblies.

### 2.3. CO<sub>2</sub> Stimulus Responsiveness

In view of these promising results, we envisaged that the soft materials could experience a reversible gel-to-sol transition triggered by carbon dioxide. It is well-known that the solubility of carbon dioxide in water leads to a noteworthy decrease in the pH, reaching values between 3.5 and 4 [53]. In addition, amines have been widely used as chemical absorbents of carbon dioxide [54]. The interaction of CO<sub>2</sub> with unhindered primary amines is known to generate ammonium carbamate species, because primary amines are more basic and nucleophilic than water [55,56].

We performed <sup>1</sup>H NMR analyses using DMSO-*d*<sub>6</sub> as the solvent to obtain information about the formation of ammonium carbamate products [57]. For comparison, the spectrum of the diprotonated (**6b**·2HCl) species in DMSO was also recorded. Significant differences were observed when comparing the spectra of freshly prepared **6b** with the one of (**6b**·2HCl) and that of **6b** after bubbling a CO<sub>2</sub> balloon for 5 min (Figure S10). For **6b**-CO<sub>2</sub>, the downfield shift for the proton of the stereogenic carbon (from  $\delta = 3.42$  to 4.10 ppm), together with the appearance of new signals at 6.62, 8.24, and 8.59 ppm, could indicate the formation of the ammonium carbamate derivative. While the methylene protons of the central spacer shifted towards lower  $\delta$  values for (**6b**·2HCl), no shift was observed for **6b**-CO<sub>2</sub>. Furthermore, a significant downfield shift of the aromatic protons and an increase in the anisochrony of the benzylic protons was observed for **6b**-CO<sub>2</sub>, with the latter being attributed to the lack of free rotation. As expected, the signals of these CO<sub>2</sub>-derived species decreased with time, even at room temperature, indicating that the interaction with carbon dioxide was reversible (see Figure S11). This quite fast dynamic equilibrium in the NMR tube precluded its study by <sup>13</sup>C NMR. Two main approaches have been established in the literature for the formation of carbamate derivatives from diamino compounds: intramolecular asymmetric carbamate salts (Figure S12a), and dimeric symmetric carbamate species (Figure S12b) [55]. As the <sup>1</sup>H NMR spectrum of **6b** in the presence of CO<sub>2</sub> did not reflect a complex mixture of asymmetric signals, the formation of the dimeric symmetric ammonium carbamate species could be considered.

When CO<sub>2</sub> was bubbled into the **6b** gel sample (1 mg/mL in H<sub>2</sub>O:DMSO, 90:10 *v/v*), a transition from a gel to a weak gel was clearly observed by vial inversion, and the gel could not be restored after resting the vial for 24 h. The pH before and after the CO<sub>2</sub> adsorption was 8.5 and 5.4, respectively. Thus, by selecting an appropriate pH indicator, it was possible to design a colorimetric probe for the gel-sol transition. The gelation of an aqueous solution of methyl red in DMSO (10% *v/v*) with **6b** (1 mg/mL) led to the expected yellowish gel (Figure 6a—left). After bubbling in the carbon dioxide, a change in the colour of the

sample was observed, shifting from yellow to orange (Figure 6a—right). In addition, when comparing the rheological properties of a freshly prepared **6b** gel (1 mg/mL in H<sub>2</sub>O:DMSO 90:10 *v/v*) and the sample after CO<sub>2</sub> absorption, the storage modulus ( $G'$ ) decreased by more than one order of magnitude. The complex viscosity presented an average value of 5.2 Pa·s, which is more than 20 times smaller than the viscosity of the original gel (113 Pa·s). The formation of a weaker CO<sub>2</sub>-absorbed soft material was also corroborated with the values of the oscillation strain required for breaking down the gel. Whereas an oscillation strain of 10 Pa was necessary for the gel–liquid transition in the freshly prepared gel, a strain of only 0.7 Pa was necessary for the ammonium carbamate-derived sample (Figure 6b).

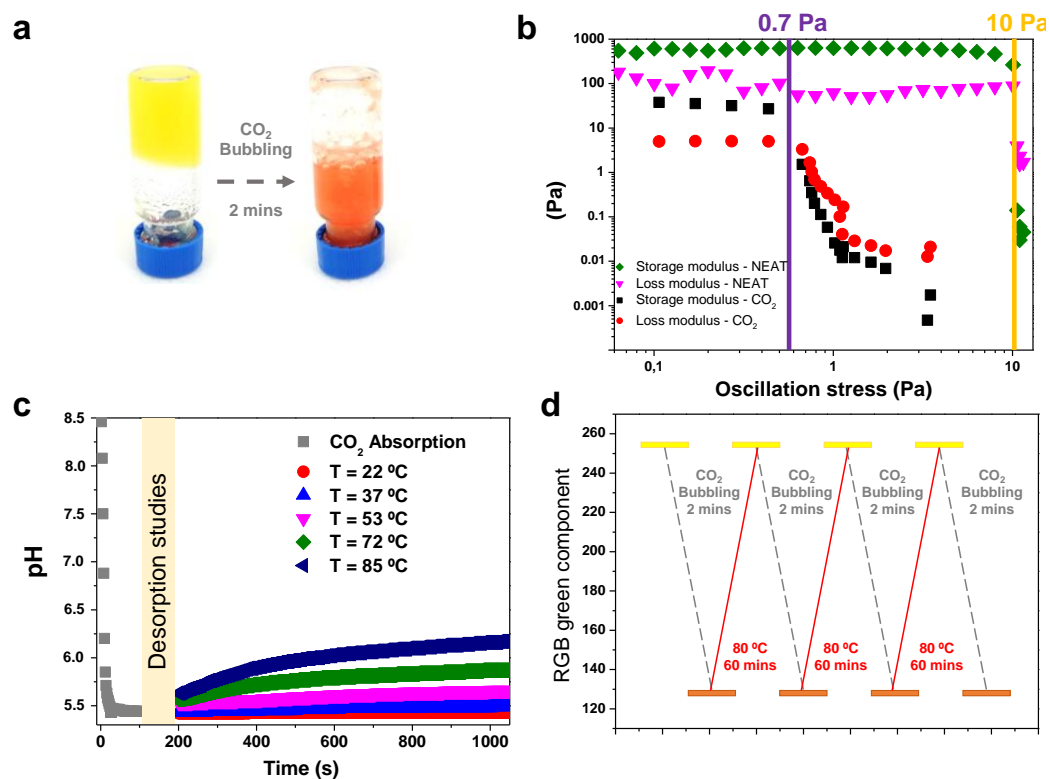


**Figure 6.** (a) A vial inversion test for the methyl red with the samples before (left) and after (right) CO<sub>2</sub> incorporation (1 mg of **6b** in 1 mL of H<sub>2</sub>O(methyl red):DMSO (90:10)). (b) The storage and loss modulus representation for neat (green and pink, respectively) and CO<sub>2</sub>-rich (black and red, respectively) samples; the oscillation stress required for the gel-to-liquid transition is highlighted in purple for the CO<sub>2</sub>-rich sample and in orange for the freshly prepared **6b** hydrogel. (c) CO<sub>2</sub> absorption/desorption results obtained via in-line monitoring of the pH for the **6b** gel (1 mg in 1 mL of H<sub>2</sub>O:DMSO, 90:10). (d) Cycles for the CO<sub>2</sub> absorption/desorption–hydrogel depletion/formation obtained for **6b** by measuring the RGB green component observed (1 mg of **6b** in 1 mL of H<sub>2</sub>O:DMSO, 90:10).

Generally, the desorption of CO<sub>2</sub> is controlled by temperature for most of the systems reported to date. This is the consequence of ammonium carbamate decomposition at high temperatures, which releases carbon dioxide and the free amino groups [58]. We speculated whether our bioinspired materials could promote hydrogel recovery upon increasing temperatures. The CO<sub>2</sub> absorption was conducted at 25 °C under atmospheric conditions and the desorption was carried out at temperatures between 30 and 80 °C. To precisely study the reversibility of the system, we determined the desorption temperature by in situ pH measurements for the sample. The pH of the gel drastically decreased from 8.5 to 5.4 in less than 100 s upon CO<sub>2</sub> bubbling. At the same time, the viscosity of the system was clearly reduced after the addition of carbon dioxide. Once the gel had been depleted, we studied the pH variations at different temperatures, providing an insight into the CO<sub>2</sub> desorption efficiency (Figure 6c). Interestingly, at temperatures > 70 °C, a significant increase in pH

was observed, indicating the decomposition of the carbamate species. To our delight, this system was thus able to promote CO<sub>2</sub> desorption at relatively low temperatures, considering that the ammonium carbamate species were formed from primary amino groups [41]. The efficient CO<sub>2</sub> release was assigned to the thermodynamically favoured recovery of the supramolecular hydrogel.

Subsequently, we designed a suitable cycle for studying the hydrogel destruction/formation using CO<sub>2</sub> as an external stimulus, obtaining promising results in terms of reversibility (Figure 6d). The experiment relied on simple colorimetric analyses using methyl orange as a pH indicator. An orange weak gel was observed after the CO<sub>2</sub> absorption, resulting in a RGB green component value of 128. Contrarily, a yellowish colour (RGB green component = 255) was observed when the hydrogel was recovered after heating at 80 °C for 60 min.

Hence, the formation of the carbamate species clearly affected the outcome of the self-assembly of the pseudopeptide. We calculated the most stable conformation for the proposed ammonium carbamate symmetric dimeric derivatives at the MMFFaq level of theory. Interestingly, although some intermolecular hydrogen-bonding interactions were found between the amide groups and the carbamate scaffolds, only one intermolecular  $\pi$ - $\pi$  interaction was detected, which supported the hypothesis that such aromatic forces are essential for achieving a supramolecular 3D network (Figure S13a). The dimeric ammonium carbamate derivative displayed a tight electrostatic interaction between the terminal ammonium and carbamate groups (Figure S13b), leading to the formation of discrete supramolecular architectures. Furthermore, the salts formed upon exposure to carbon dioxide possessed a higher solubility in water, decreasing the self-assembly efficiency (Figure S13c).

### 3. Conclusions

Novel open-chain pseudopeptides were successfully synthesized. These bioinspired species demonstrated promising properties as low-molecular-weight hydrogelators, with CGC values as low as 0.6 mg/mL. The nature of the supramolecular interactions governing gel formation was elucidated, revealing a strong cooperativity between hydrogen-bonding and  $\pi$ - $\pi$  forces. Modifications to the side chain composition and the aliphatic spacer length allowed for the modulation of the properties of the final materials. The presence of terminal amino groups in their basic form was found to be crucial for efficient self-assembly. Sol-gel transitions could be easily triggered by pH modification, obtaining the toughest materials under basic conditions (pH > 8). In addition, the high tendency of primary amines to react with carbon dioxide permitted the CO<sub>2</sub> responsiveness of these soft materials to be assayed. In this regard, remarkable results were obtained with desorption temperatures of ca. 70 °C, which were assigned to the thermodynamically favoured recovery of the supramolecular gel.

### 4. Materials and Methods

#### 4.1. General

The reagents and solvents were purchased from commercial suppliers and used without further purification. Deionized water was obtained from MilliQ (Burlington, MA, USA).

The NMR experiments were carried out on a Varian INOVA 500 spectrometer (Mundelein, IL, USA, 500 MHz for <sup>1</sup>H and 125 MHz for <sup>13</sup>C), on a Bruker 400 (400 MHz for <sup>1</sup>H and 100 MHz for <sup>13</sup>C), or on a Bruker 300 (300 MHz for <sup>1</sup>H and 75 MHz for <sup>13</sup>C). Chemical shifts were reported in parts per million using the solvent's residual peak as the reference.

ATR FT-IR spectra were acquired using a JASCO 6200 device with a MIRacle Single Reflection ATR Diamond/ZnSe accessory. The samples were directly deposited onto the ATR sample holder, and the FT-IR spectra were collected. The raw IR data were processed with JASCO spectral manager software (Version 2).

UV–Vis absorption measurements were carried out on a Hewlett–Packard 8453 spectrophotometer (Palo Alto, CA, USA) with a controlled temperature system.

#### 4.2. Gelation Experiments

In a typical experiment, a weighted amount of the LMWG was mixed with 1 mL of the selected solvent in a 1.5 mL glass vial. Gelation was defined when a homogeneous mixture was obtained that exhibited no gravitational flow upon inversion of the vial. For organic/water solvent mixtures, the LMWG was first dissolved in the corresponding amount of the organic solvent (DMSO or EtOH) and MilliQ water was subsequently added.

#### 4.3. Rheological Experiments

The different gels were characterized using a controlled stress AR-2000 rheometer from TA Instruments (New Castle, DE, USA). A Peltier holder with a plate geometry (60 mm diameter, 500  $\mu\text{m}$  gap) was used for all samples. Frequency sweeps were performed in the angular frequency range 0.1–100  $\text{rad s}^{-1}$  with the instrument in oscillatory mode at 25  $^{\circ}\text{C}$ . Strain sweeps were performed using a frequency of 1  $\text{rad s}^{-1}$  in an amplitude sweep range of 0.01–80% with the instrument in oscillatory mode at 25  $^{\circ}\text{C}$ .

#### 4.4. Molecular Modelling

The lowest energy conformations for the different species considered were calculated at the MMFFaq level of theory using Spartan08 [59]. The stationary points were confirmed by subsequent frequency calculation. All vibrational frequencies were positive. See the supporting information for the Cartesian coordinates.

#### 4.5. Synthetic Protocols

The  $C_2$ -symmetrical bis(aminoamides) (**4**) were prepared as previously reported [44].

##### 4.5.1. Synthesis of Cbz-N Protected Tetra-Pseudopeptidic Intermediates (**5**) Synthesis of **5a**

The compound **2a** (7.741 g, 10.686 mmol) was dissolved in anhydrous DME (150 mL) at 0  $^{\circ}\text{C}$  in a two-necked round-bottomed flask (500 mL) using a  $\text{N}_2$  atmosphere. A DME solution (150 mL) of **4a** (3.02 g, 11 mmol) was then added dropwise. The reaction mixture was stirred at 0  $^{\circ}\text{C}$  for 1 h and at 25  $^{\circ}\text{C}$  for 18 h. Subsequently, the white suspension was heated for 6 h at 40–50  $^{\circ}\text{C}$ . The resultant white precipitate was filtered off and washed with cold water and cold methanol. The solid product was dried overnight under reduced pressure at 50  $^{\circ}\text{C}$  to yield **5a** as a white solid. The yield was 7.09 g (9.79 mmol, 89.0%). The product was used for the subsequent step without further purification.

##### Synthesis of **5b**

Intermediate **5b** was successfully synthesized following the same procedure as described for **5a**, but using **2b** instead of **2a** and **4b** instead of **4a**. The yield was 3.473 g (3.804 mmol, 87.0%). The product was used for the subsequent step without further purification.

##### Synthesis of **5c**

Intermediate **5c** was successfully synthesized following the same procedure as described for **5a**, but using **2b** instead of **2a** and **4c** instead of **4a**. The yield was 3.186 g (3.330 mmol, 76.9%). The product was used for the subsequent step without further purification.

##### Synthesis of **5d**

Intermediate **5d** was successfully synthesized following the same procedure as described for **5a**, but using **2b** instead of **2a** and **4d** instead of **4a**. The yield was 2.209 g (2.192 mmol, 81.6%). The product was used for the subsequent step without further purification.

### Synthesis of 5e

Intermediate **5e** was successfully synthesized following the same procedure as described for **5a**, but using **2b** instead of **2a**. The yield was 4.931 g (6.001 mmol, 90.9%). The product was used for the subsequent step without further purification.

### Synthesis of 5f

Intermediate **5f** was successfully synthesized following the same procedure as described for **5a**, but using **4b** instead of **4a**. The yield was 1.238 g (1.506 mmol, 63.2%). The product was used for the subsequent step without further purification.

## 4.5.2. Synthesis of Tetra-Pseudopeptidic Compounds (6)

### Synthesis of 6a

The compound **5a** (0.676 g, 0.932 mmol) was suspended in methanol (150 mL) in a 250 mL two-necked round-bottomed flask using an ultrasonic bath. After obtaining a N<sub>2</sub> atmosphere, Pd/C (0.198 g, 0.092 mmol) was poured into the flask while nitrogen was being flushed. The nitrogen balloons were then replaced by ones filled with hydrogen and the mixture was stirred for 24 h. The suspension was filtered through a Celite<sup>®</sup> layer, and the adsorbent was washed with methanol. The final solution was evaporated under reduced pressure to yield pure **6a** as a white solid. The yield was 0.346 g (0.758 mmol, 81.3%); the mp was 228–229 °C;  $[\alpha]_{\text{D}}^{25} = -7.32^{\circ}$  ( $c = 0.1$ , DMSO); ATR-FTIR: 3278, 3050, 1634, and 1537 cm<sup>-1</sup>; <sup>1</sup>H NMR (400 MHz, CD<sub>3</sub>OD)  $\delta = 0.85\text{--}0.99$  (m, 24H), 1.95 (m, 4H), 3.08 (t,  $J = 14.94$ , 14.94 Hz, 2H), 3.17 (dd,  $J = 5.46$ , 14.16 Hz, 2H), 3.24 (d,  $J = 6.55$  Hz, 2H), and 4.01 (d,  $J = 7.07$  Hz, 2H); <sup>13</sup>C{<sup>1</sup>H} NMR (75 MHz, CD<sub>3</sub>OD)  $\delta = 16.1$ , 17.3, 18.4, 18.5, 30.4, 31.8, 38.6, 58.8, 60.1, 172.6, and 175.8; HRMS (ESI/Q-TOF)  $m/z$ : [M + H]<sup>+</sup> calculated for C<sub>22</sub>H<sub>44</sub>N<sub>6</sub>O<sub>4</sub> 457.3502; found 457.3498.

### Synthesis of 6b

The compound **6b** was successfully synthesized following the same procedure as described for **6a**, but using **5b** instead of **5a**. The yield was 0.331 g (0.510 mmol, 82.5%); the mp was 193–195 °C;  $[\alpha]_{\text{D}}^{25} = -3.42^{\circ}$  ( $c = 0.05$ , DMSO); ATR-FTIR: 3282, 3042, 1648, and 1535 cm<sup>-1</sup>; <sup>1</sup>H NMR (300 MHz, CD<sub>3</sub>OD)  $\delta = 2.41\text{--}3.13$  (m, 12H), 3.40–3.51 (m, 2H), 4.36–4.48 (m, 2H), and 6.95–7.29 (m, 20H); <sup>13</sup>C{<sup>1</sup>H} NMR (75 MHz, CD<sub>3</sub>OD)  $\delta = 37.6$ , 38.7, 40.3, 54.5, 56.0, 126.4, 126.5, 128.1, 128.2, 129.0, 129.0, 136.9, 137.3, 172.3, and 175.0; HRMS (ESI/Q-TOF)  $m/z$ : [M + H]<sup>+</sup> calculated for C<sub>38</sub>H<sub>44</sub>N<sub>6</sub>O<sub>4</sub> 649.3502; found 649.3508.

### Synthesis of 6c

The compound **6c** was successfully synthesized following the same procedure as described for **6a**, but using **5c** instead of **5a**. The yield was 1.269 g (1.837 mmol, 78.4%); the mp was 152–154 °C;  $[\alpha]_{\text{D}}^{25} = -6.21^{\circ}$  ( $c = 0.05$ , DMSO); ATR-FTIR: 3283, 3042, 1639, and 1529 cm<sup>-1</sup>; <sup>1</sup>H NMR (400 MHz, CD<sub>3</sub>OD)  $\delta = 0.99$  (tt,  $J = 10.2$ , 6.3 Hz, 2H), 1.16–1.30 (m, 4H), 2.50–2.64 (m, 2H), 2.75–3.03 (m, 10H), 3.44 (dd,  $J = 7.8$ , 5.4 Hz, 2H), 4.45 (t,  $J = 7.4$  Hz, 2H), and 7.21–7.01 (m, 20H); <sup>13</sup>C{<sup>1</sup>H} NMR (100 MHz, CD<sub>3</sub>OD)  $\delta = 25.0$ , 29.8, 39.4, 40.2, 42.0, 55.8, 57.4, 127.8, 127.9, 129.5, 129.6, 130.5, 138.2, 138.8, 172.9, and 176.5; HRMS (ESI/Q-TOF)  $m/z$ : [M + H]<sup>+</sup> calculated for C<sub>41</sub>H<sub>50</sub>N<sub>6</sub>O<sub>4</sub> 691.3972; found 691.3973.

### Synthesis of 6d

The compound **6d** was successfully synthesized following the same procedure as described for **6a**, but using **5d** instead of **5a**. The yield was 0.485 g (0.662 mmol, 70.1%); the mp was 138–141 °C;  $[\alpha]_{\text{D}}^{25} = -3.02^{\circ}$  ( $c = 0.05$ , DMSO); ATR-FTIR: 3272, 3085, 1654, and 1542 cm<sup>-1</sup>; <sup>1</sup>H NMR (400 MHz, CD<sub>3</sub>OD)  $\delta = 1.01\text{--}1.18$  (m, 10H), 1.26 (p,  $J = 7.7$ , 6.9 Hz, 4H), 2.51–2.65 (m, 2H), 2.76–3.03 (m, 10H), 3.44 (dd,  $J = 7.7$ , 5.5 Hz, 2H), 4.45 (t,  $J = 7.3$  Hz, 2H), and 7.20–7.01 (m, 10H); <sup>13</sup>C{<sup>1</sup>H} NMR (100 MHz, CD<sub>3</sub>OD)  $\delta = 27.8$ , 30.2, 39.4, 40.4, 42.1, 55.8, 57.4, 127.8, 127.9, 129.5, 129.6, 130.5, 138.2, 138.8, 172.3, and 176.5; HRMS (ESI/Q-TOF)  $m/z$ : [M + H]<sup>+</sup> calculated for C<sub>44</sub>H<sub>56</sub>N<sub>6</sub>O<sub>4</sub> 733.4441; found 733.4449.

### Synthesis of 6e

The compound **6e** was successfully synthesized following the same procedure as described for **6a**, but using **5e** instead of **5a**. The yield was 0.263 g (0.475 mmol, 77.4%); the mp was 207–209 °C;  $[\alpha]_D^{25} = -1.75^\circ$  ( $c = 0.05$ , DMSO); ATR-FTIR: 3280, 3085, 1636, and 1546  $\text{cm}^{-1}$ ;  $^1\text{H}$  NMR (400 MHz, DMSO- $d_6$ )  $\delta = 0.80$  (dd,  $J = 6.8, 5.0$  Hz, 6H), 1.92 (h,  $J = 6.6$  Hz, 2H), 2.63 (dd,  $J = 13.4, 8.5$  Hz, 2H), 2.99 (dd,  $J = 13.5, 4.3$  Hz, 2H), 3.11 (s, 4H), 3.46 (dd,  $J = 8.6, 4.3$  Hz, 2H), 4.10 (t,  $J = 7.3$  Hz, 2H), 7.38–7.14 (m, 10H), 7.96 (d,  $J = 9.0$  Hz, 2H), and 8.03 (s, 2H);  $^{13}\text{C}\{^1\text{H}\}$  NMR (100 MHz, DMSO- $d_6$ )  $\delta = 18.5, 19.6, 31.3, 41.1, 56.5, 57.7, 126.6, 128.6, 129.8, 139.1, 171.4, \text{ and } 174.4$ ; HRMS (ESI/Q-TOF)  $m/z$ :  $[\text{M} + \text{H}]^+$  calculated for  $\text{C}_{30}\text{H}_{44}\text{N}_6\text{O}_4$  553.3497; found 553.3503.

### Synthesis of 6f

The compound **6f** was successfully synthesized following the same procedure as described for **6a**, but using **5f** instead of **5a**. The yield was 0.428 g (0.774 mmol, 63.5%); the mp was 184–189 °C;  $[\alpha]_D^{25} = -8.2^\circ$  ( $c = 0.05$ , DMSO); ATR-FTIR: 3282, 3083, 1636, and 1535  $\text{cm}^{-1}$ ;  $^1\text{H}$  NMR (300 MHz, DMSO- $d_6$ )  $\delta = 0.56$  (dd,  $J = 6.8, 1.5$  Hz, 6H), 0.73 (d,  $J = 6.9$  Hz, 6H), 1.81 (tdd,  $J = 6.8, 4.7, 2.0$  Hz, 2H), 2.58 (dd,  $J = 13.3, 8.3$  Hz, 2H), 2.76–2.88 (m, 2H), 2.91–2.97 (m, 4H), 3.04 (d,  $J = 3.2$  Hz, 2H), 4.43–4.52 (m, 2H), 7.18–7.27 (m, 10H), 7.90 (d,  $J = 5.9$  Hz, 2H), and 8.05 (s, 2H);  $^{13}\text{C}\{^1\text{H}\}$  NMR (75 MHz, DMSO- $d_6$ )  $\delta = 17.0, 17.1, 19.9, 31.5, 38.5, 126.7, 128.5, 129.6, 138.2, 171.6, \text{ and } 174.7$ ; HRMS (ESI/Q-TOF)  $m/z$ :  $[\text{M} + \text{H}]^+$  calculated for  $\text{C}_{30}\text{H}_{44}\text{N}_6\text{O}_4$  553.3497; found 553.3508.

**Supplementary Materials:** The following supporting information can be downloaded at: <https://www.mdpi.com/article/10.3390/gels8060390/s1>: Table S1: CGC results by vial inversion; Figure S1: Vial inversion images for determining CGC; Table S2: Thermal stability results using vial inversion; Figure S2: Rheological measurements for **6b** (5 mg/mL); Figure S3: pH dependence vial inversion tests; Figure S4: SEM images for (**6b**·2HCl) crystals; Figure S5: Partial  $^1\text{H}$  NMR spectra for **6b** titration with  $\text{H}_2\text{O}$ ; Figure S6: Partial  $^1\text{H}$  NMR spectra for **6b** and **6f** titrations with  $\text{H}_2\text{O}$ ; Figure S7: Partial  $^1\text{H}$  NMR spectra (aromatic region) for **6b** and **6f** titrations with  $\text{H}_2\text{O}$ ; Figure S8: Variable temperature  $^1\text{H}$  NMR spectra; Figure S9: MMFFaq non-covalent forces **6b**-dimer; Figure S10: Partial  $^1\text{H}$  NMR spectra for  $\text{CO}_2$  absorption with **6b**; Figure S11: Time evolution  $^1\text{H}$  NMR spectra for  $\text{CO}_2$  absorption with **6b**; Figure S12: Main approaches for carbamate formation with diamines; Figure S13: Molecular models for ammonium carbamate **6b**- $\text{CO}_2$  species; spectroscopic characterization, cartesian coordinates.

**Author Contributions:** Conceptualization, F.E. and B.A.; data curation, F.E. and A.V.-A.; formal analysis, F.E. and B.A.; investigation, F.E. and A.V.-A.; funding acquisition, B.A., E.G.-V. and S.V.L.; project administration, B.A. and S.V.L.; resources, B.A., E.G.-V. and S.V.L.; writing—original draft, F.E.; writing—review and editing, F.E., B.A., E.G.-V. and S.V.L. All authors have read and agreed to the published version of the manuscript.

**Funding:** This research was funded by Universitat Jaume I, grant number UJI-B2019-40 and UJI-B2021-31; Conselleria de Innovació, Universitat, i Ciència, grant number AICO/2021/139; and FEDER/Ministerio de Ciencia e Innovación–Agencia Estatal de Investigación, grant number RTI2018-098233-B-C22.

**Institutional Review Board Statement:** Not applicable.

**Informed Consent Statement:** Not applicable.

**Data Availability Statement:** Not applicable.

**Acknowledgments:** F.E. acknowledges MECED for a FPU fellowship (FPU 2017/02060). Technical support from the SCIC of the UJI is gratefully acknowledged.

**Conflicts of Interest:** The authors declare no conflict of interest.

## References and Note

1. Dastidar, P. Supramolecular gelling agents: Can they be designed? *Chem. Soc. Rev.* **2008**, *37*, 2699–2715. [[CrossRef](#)] [[PubMed](#)]
2. Buerkle, L.E.; Rowan, S. Supramolecular gels formed from multi-component low molecular weight species. *Chem. Soc. Rev.* **2012**, *41*, 6089–6102. [[CrossRef](#)] [[PubMed](#)]
3. Draper, E.R.; Adams, D.J. How should multicomponent supramolecular gels be characterised? *Chem. Soc. Rev.* **2018**, *47*, 3395–3405. [[CrossRef](#)] [[PubMed](#)]
4. Chivers, P.R.A.; Smith, D.K. Shaping and structuring supramolecular gels. *Nat. Rev. Mater.* **2019**, *4*, 463–478. [[CrossRef](#)]
5. Levin, A.; Hakala, T.A.; Schnaider, L.; Bernardes, G.J.L.; Gazit, E.; Knowles, T.P.J. Biomimetic peptide self-assembly for functional materials. *Nat. Rev. Chem.* **2020**, *4*, 615–634. [[CrossRef](#)]
6. Wang, D.X.; Wang, M.X. Exploring Anion– $\pi$  Interactions and Their Applications in Supramolecular Chemistry. *Acc. Chem. Res.* **2020**, *53*, 1364–1380. [[CrossRef](#)] [[PubMed](#)]
7. Stankovic, I.M.; Niu, S.Q.; Hall, M.B.; Zaric, S.O. Role of aromatic amino acids in amyloid self-assembly. *Int. J. Biol. Macromol.* **2020**, *156*, 949–959. [[CrossRef](#)] [[PubMed](#)]
8. Piras, C.C.; Smith, D.K. Sequential Assembly of Mutually Interactive Supramolecular Hydrogels and Fabrication of Multi-Domain Materials. *Chem. Eur. J.* **2019**, *25*, 11318–11326. [[CrossRef](#)]
9. Cheng, W.; Ding, Z.; Zheng, X.; Lu, Q.; Kong, X.; Zhou, X.; Lumand, G.; Kaplan, D.L. Injectable hydrogel systems with multiple biophysical and biochemical cues for bone regeneration. *Biomater. Sci.* **2020**, *8*, 2537–2548. [[CrossRef](#)]
10. Li, Z.; Huang, J.; Wu, J. pH-Sensitive nanogels for drug delivery in cancer therapy. *Biomater. Sci.* **2021**, *9*, 574–589. [[CrossRef](#)]
11. Hoffman, A.S. Hydrogels for biomedical applications. *Adv. Drug Delivery Rev.* **2012**, *64*, 18–23. [[CrossRef](#)]
12. Mayr, J.; Saldias, C.; Diaz, D.D. Release of small bioactive molecules from physical gels. *Chem. Soc. Rev.* **2018**, *47*, 1484–1515. [[CrossRef](#)] [[PubMed](#)]
13. Guo, V.H.; Bae, J.; Fang, Z.W.; Li, P.P.; Zhao, F.; Vu, G.H. Hydrogels and Hydrogel-Derived Materials for Energy and Water Sustainability. *Chem. Rev.* **2020**, *120*, 7642–7707. [[CrossRef](#)] [[PubMed](#)]
14. Chen, J.A.; Leung, F.K.C.; Stuart, M.C.A.; Kajitani, T.; Fukushima, T.; van der Giessen, E.; Feringa, B.L. Artificial muscle-like function from hierarchical supramolecular assembly of photoresponsive molecular motors. *Nat. Chem.* **2018**, *10*, 132–138. [[CrossRef](#)] [[PubMed](#)]
15. Nele, V.; Wojciechowski, J.P.; Armstrong, J.P.K.; Stevens, M.M. Tailoring Gelation Mechanisms for Advanced Hydrogel Applications. *Adv. Funct. Mater.* **2020**, *30*, 2002759. [[CrossRef](#)]
16. Fleming, S.; Ulijn, R.V. Design of nanostructures based on aromatic peptide amphiphiles. *Chem. Soc. Rev.* **2014**, *43*, 8150–8177. [[CrossRef](#)]
17. Dou, X.-Q.; Feng, C.-L. Amino Acids and Peptide-Based Supramolecular Hydrogels for Three-Dimensional Cell Culture. *Adv. Mater.* **2017**, *29*, 1604062. [[CrossRef](#)]
18. Ramalheite, S.M.; Nartowski, K.P.; Sarathchandra, N.; Foster, J.S.; Round, A.N.; Angulo, J.; Lloyd, G.O.; Khimyak, Y.Z. Supramolecular Amino Acid Based Hydrogels: Probing the Contribution of Additive Molecules using NMR Spectroscopy. *Chem. Eur. J.* **2017**, *23*, 8014–8024. [[CrossRef](#)]
19. Das, T.; Häring, M.; Haldar, D.; Díaz, D.D. Phenylalanine and derivatives as versatile low-molecular-weight gelators: Design, structure and tailored function. *Biomater. Sci.* **2018**, *6*, 38–59. [[CrossRef](#)]
20. Giraud, T.; Hoschtettler, P.; Pickaert, G.; Averlant-Petit, M.-C.; Stefan, L. Emerging low-molecular weight nucleopeptide-based hydrogels: State of the art, applications, challenges and perspectives. *Nanoscale* **2022**, *14*, 4908–4921. [[CrossRef](#)]
21. Ulijn, R.V.; Smith, A.M. Designing peptide based nanomaterials. *Chem. Soc. Rev.* **2008**, *37*, 664–675. [[CrossRef](#)] [[PubMed](#)]
22. Zanna, N.; Merlettini, A.; Tomasini, C. Self-healing hydrogels triggered by amino acids. *Org. Chem. Front.* **2016**, *3*, 1699–1704. [[CrossRef](#)]
23. Steed, J.W. Anion-tuned supramolecular gels: A natural evolution from urea supramolecular chemistry. *Chem. Soc. Rev.* **2010**, *39*, 3686–3699. [[CrossRef](#)] [[PubMed](#)]
24. Valls, A.; Castillo, A.; Porcar, R.; Hietala, S.; Altava, B.; García-Verdugo, E.; Luis, S.V. Urea-Based Low-Molecular-Weight Pseudopeptidic Organogelators for the Encapsulation and Slow Release of (R)-Limonene. *J. Agric. Food Chem.* **2020**, *68*, 7051–7061. [[CrossRef](#)]
25. Rubio, J.; Alfonso, I.; Burguete, M.I.; Luis, S.V. Interplay between hydrophilic and hydrophobic interactions in the self-assembly of a gemini amphiphilic pseudopeptide: From nano-spheres to hydrogels. *Chem. Commun.* **2012**, *48*, 2210–2212. [[CrossRef](#)]
26. Valls, A.; Burguete, M.I.; Kuret, L.; Altava, B.; Luis, S.V. Open chain pseudopeptides as hydrogelators with reversible and dynamic responsiveness to pH, temperature and sonication as vehicles for controlled drug delivery. *J. Mol. Liq.* **2022**, *348*, 118051. [[CrossRef](#)]
27. Raza, F.; Zhu, Y.; Chen, L.; You, X.; Zhang, J.; Khan, A.; Waseem Khan, M.; Hasnat, M.; Zafar, H.; Wu, J.; et al. Paclitaxel-loaded pH responsive hydrogel based on self-assembled peptides for tumor targeting. *Biomater. Sci.* **2019**, *7*, 2023–2036. [[CrossRef](#)]
28. Cardoso, A.Z.; Alvarez, A.E.A.; Cattoz, B.N.; Griffiths, P.C.; King, S.M.; Frith, W.J.; Adams, D.J. The influence of the kinetics of self-assembly on the properties of dipeptide hydrogels. *Faraday Discuss.* **2013**, *166*, 101–116. [[CrossRef](#)]
29. Shaikh, H.; Rho, J.Y.; Macdougall, L.J.; Gurnani, P.; Lunn, A.M.; Yang, J.; Huband, S.; Mansfield, E.D.H.; Peltier, R.; Perrier, S. Hydrogel and Organogel Formation by Hierarchical Self-Assembly of Cyclic Peptides Nanotubes. *Chem. Eur. J.* **2018**, *24*, 19066–19074. [[CrossRef](#)]

30. Chu, C.-W.; Stricker, L.; Kirse, T.M.; Hayduk, M.; Ravoo, B.J. Light-Responsive Arylazopyrazole Gelators: From Organic to Aqueous Media and from Supramolecular to Dynamic Covalent Chemistry. *Chem. Eur. J.* **2019**, *25*, 6131–6140. [[CrossRef](#)]
31. Wang, H.; Heilshorn, S.C. Adaptable Hydrogel Networks with Reversible Linkages for Tissue Engineering. *Adv. Mater.* **2015**, *27*, 3717. [[CrossRef](#)] [[PubMed](#)]
32. Chen, W.H.; Liao, W.-C.; Sohn, Y.S.; Fadeev, M.; Ceconello, A.; Nechushtai, R.; Willner, I. Stimuli-Responsive Nucleic Acid-Based Polyacrylamide Hydrogel-Coated Metal–Organic Framework Nanoparticles for Controlled Drug Release. *Adv. Funct. Mater.* **2018**, *28*, 1705137. [[CrossRef](#)]
33. Doring, A.; Birnbaum, W.; Kuckling, D. Responsive hydrogels—Structurally and dimensionally optimized smart frameworks for applications in catalysis, micro-system technology and material science. *Chem. Soc. Rev.* **2013**, *42*, 7391–7420. [[CrossRef](#)] [[PubMed](#)]
34. Han, D.; Boissiere, O.; Kumar, S.; Tong, X.; Tremblay, L.; Zhao, Y. Two-Way CO<sub>2</sub>-Switchable Triblock Copolymer Hydrogels. *Macromolecules* **2012**, *45*, 7440–7445. [[CrossRef](#)]
35. Zhang, L.; Qian, J.; Fan, Y.; Feng, W.; Tao, Z.; Yang, H. A facile CO<sub>2</sub> switchable nanocomposite with reversible transition from sol to self-healable hydrogel. *RSC Adv.* **2015**, *5*, 62229–62234. [[CrossRef](#)]
36. Jie, K.; Zhou, Y.; Yao, Y.; Shi, B.; Huang, F. CO<sub>2</sub>-Responsive Pillar[5]arene-Based Molecular Recognition in Water: Establishment and Application in Gas-Controlled Self-Assembly and Release. *J. Am. Chem. Soc.* **2015**, *137*, 10472–10475. [[CrossRef](#)]
37. Nagasawa, Y.; Seida, Y.; Gotoh, T.; Furuya, E. Influence of Hydrophobicity of Backbone Polymer in Thermo-Responsive Hydrogel with Immobilized Amine on Cycle Capacity for Absorption and Recovery of CO<sub>2</sub>. *Polymers* **2019**, *11*, 1024. [[CrossRef](#)] [[PubMed](#)]
38. Jia, Y.G.; Zhang, M.; Zhu, X.X. CO<sub>2</sub>-Switchable Self-Healing Host–Guest Hydrogels. *Macromolecules* **2017**, *50*, 9696–9701. [[CrossRef](#)]
39. Satav, S.S.; Bhat, S.; Thayumanavan, S. Feedback Regulated Drug Delivery Vehicles: Carbon Dioxide Responsive Cationic Hydrogels for Antidote Release. *Biomacromolecules* **2010**, *11*, 1735–1740. [[CrossRef](#)] [[PubMed](#)]
40. George, M.; Weiss, R.G. Chemically Reversible Organogels: Aliphatic Amines as “Latent” Gelators with Carbon Dioxide. *J. Am. Chem. Soc.* **2001**, *123*, 10393–10394. [[CrossRef](#)]
41. Rao, A.B.; Rubin, E.S. A Technical, Economic, and Environmental Assessment of Amine-Based CO<sub>2</sub> Capture Technology for Power Plant Greenhouse Gas Control. *Environ. Sci. Technol.* **2002**, *36*, 4467–4475. [[CrossRef](#)] [[PubMed](#)]
42. Allix, F.; Curcio, P.; Nghi Pham, Q.; Pickaert, G.; Jamart-Gregoire, B. Evidence of Intercolumnar  $\pi$ – $\pi$  Stacking Interactions in Amino-Acid-Based Low-Molecular-Weight Organogels. *Langmuir* **2010**, *26*, 16818–16827. [[CrossRef](#)] [[PubMed](#)]
43. Ghosh, S.; Adler-Abramovich, L.; Gazit, E.; Verma, S. Spacer driven morphological twist in Phe-Phe dipeptide conjugates. *Tetrahedron* **2013**, *69*, 2004–2009. [[CrossRef](#)]
44. Becerril, J.; Bolte, M.; Burguete, M.I.; Galindo, F.; García-España, E.; Luis, S.V.; Miravet, J.F. Efficient Macrocyclization of U-Turn Preorganized Peptidomimetics: The Role of Intramolecular H-Bond and Solvophobic Effects. *J. Am. Chem. Soc.* **2003**, *125*, 6677–6686. [[CrossRef](#)] [[PubMed](#)]
45. Gorla, L.; Martí-Centelles, V.; Altava, B.; Burguete, M.I.; Luis, S.V. The role of the side chain in the conformational and self-assembly patterns of C<sub>2</sub>-symmetric Val and Phe pseudopeptidic derivatives. *CrystEngComm* **2019**, *21*, 2398–2408. [[CrossRef](#)]
46. Becerril, J.; Escuder, B.; Miravet, J.F.; Gavara, R.; Luis, S.V. Understanding the Expression of Molecular Chirality in the Self-Assembly of a Peptidomimetic Organogelator. *Eur. J. Org. Chem.* **2005**, *2005*, 481–485. [[CrossRef](#)]
47. Murata, K.; Aoki, M.; Suzuki, T.; Harada, T.; Kawabata, H.; Komori, T.; Ohseto, F.; Ueda, K.; Shinkai, S. Thermal and Light Control of the Sol-Gel Phase Transition in Cholesterol-Based Organic Gels. Novel Helical Aggregation Modes as Detected by Circular Dichroism and Electron Microscopic Observation. *J. Am. Chem. Soc.* **1994**, *116*, 6664–6676. [[CrossRef](#)]
48. Yan, C.; Pochan, D. Rheological properties of peptide-based hydrogels for biomedical and other applications. *Chem. Soc. Rev.* **2010**, *39*, 3528–3540. [[CrossRef](#)]
49. El-Husseiny, H.M.; Mady, E.A.; Hamabe, L.; Abugomaa, A.; Shimada, K.; Yoshida, T.; Tanaka, T.; Yokoi, A.; Elbadawy, M.; Tanaka, R. Smart/stimuli-responsive hydrogels: Cutting-edge platforms for tissue engineering and other biomedical applications. *Mater. Today Bio* **2022**, *13*, 100186. [[CrossRef](#)]
50. Lin, C.; Skufca, J.; Partch, R.E. New insights into prediction of weak  $\pi$ – $\pi$  complex association through proton-nuclear magnetic resonance analysis. *BMC Chem.* **2020**, *14*, 66. [[CrossRef](#)]
51. Alvarez, S. A cartography of the van der Waals territories. *Dalton Trans.* **2013**, *42*, 8617–8636. [[CrossRef](#)] [[PubMed](#)]
52. Alfonso, I.; Burguete, M.I.; Galindo, F.; Luis, S.V.; Vigarra, L. Molecular Rotors as Simple Models to Study Amide NH–Aromatic Interactions and Their Role in the Folding of Peptide-like Structures. *J. Org. Chem.* **2007**, *72*, 7947–7956. [[CrossRef](#)] [[PubMed](#)]
53. Peng, C.; Crawshaw, J.P.; Maitland, G.C.; Martin Trusler, J.P.; Vega-Mazza, D. The pH of CO<sub>2</sub>-Saturated Water at Temperatures Between 308 K and 423 K at Pressures up to 15 MPa. *J. Supercrit. Fluids* **2013**, *82*, 129–137. [[CrossRef](#)]
54. Wang, M.; Lawal, A.; Stephenson, P.; Sidders, J.; Ramshaw, C. Post-combustion CO<sub>2</sub> capture with chemical absorption: A state-of-the-art review. *Chem. Eng. Res. Des.* **2011**, *89*, 1609–1624. [[CrossRef](#)]
55. Heldebrant, D.J.; Koech, P.K.; Ang, M.T.C.; Liang, C.; Rainbolt, J.E.; Yonker, C.R.; Jessop, P.G. Reversible zwitterionic liquids, the reaction of alkanol guanidines, alkanol amidines, and diamines with CO<sub>2</sub>. *Green Chem.* **2010**, *12*, 713–721. [[CrossRef](#)]
56. Said, R.B.; Kolle, J.M.; Essalah, K.; Tangour, B.; Sayari, A. A Unified Approach to CO<sub>2</sub>–Amine Reaction Mechanisms. *ACS Omega* **2020**, *5*, 26125–26133. [[CrossRef](#)] [[PubMed](#)]
57. Note: Studies in D<sub>2</sub>O or D<sub>2</sub>O/DMSO-*d*<sub>6</sub> mixtures could not be performed due to gel formation.

- 
58. Hampe, E.M.; Rudkevich, D.M. Exploring reversible reactions between CO<sub>2</sub> and amines. *Tetrahedron* **2003**, *59*, 9619–9625. [[CrossRef](#)]
  59. Deppmeier, B.J.; Driessen, A.J.; Hehre, T.S.; Hehre, W.J.; Johnson, J.A.; Klunzinger, P.E.; Leonard, J.M.; Pham, I.N.; Pietro, W.J.; Jianguo, Y. *Calculated Using Spartan08 Software at the MMFFaq Level of Theory*; Spartan '08, build 132 (Mar 27 2009); Wavefunction Inc.: Irvine, CA, USA, 2009.